Terahertz detection using enhanced two-step absorption in photoconductive metasurfaces gated at λ=1.55 μm

Hyunseung Jung[†,], Lucy L Hale[†,*], Jayson Briscoe, Raktim Sarma, Ting Shan Luk, Sadhvikas J Addamane, John L Reno, Igal Brener, Oleg Mitrofanov[*]*

[†]These authors have contributed equally

H. Jung, J. Briscoe, R. Sarma, T. S. Luk, S. J. Addamane, J. L. Reno, I. Brener, O. Mitrofanov

Center for Integrated Nanotechnologies, Sandia National Laboratories, Albuquerque, New Mexico 87123, USA

E-mail: hjung@sandia.gov

H. Jung, J. Briscoe, R. Sarma, T. S. Luk, S. J. Addamane, J. L. Reno, I. Brener

Sandia National Laboratories, Albuquerque, New Mexico 87123, USA

L. L. Hale, O. Mitrofanov

University College London, Electronic and Electrical Engineering, London WC1E 7JE, UK

E-mail: lucy.hale@ucl.ac.uk; o.mitrofanov@ucl.ac.uk

Keywords: Terahertz, metasurface, photoconductive antenna, spectroscopy, nanofabrication

Abstract

Superior ultrafast photoconductive properties make low temperature grown (LT) GaAs one of the best materials for photoconductive terahertz (THz) detection. However, the large bandgap of LT-GaAs limits its operation to gating at wavelengths shorter than 870 nm. Here, we demonstrate for the first time that by nanostructuring the LT-GaAs into a highly absorbing metasurface we enable THz photoconductive detection with a pulsed laser at λ=1.55 μm. The very weak sub-bandgap absorption mediated by midgap states in LT-GaAs is strongly enhanced using the concept of perfect absorption via degenerate critical coupling. Integrated with a THz antenna, the LT-GaAs metasurface enables high sensitivity THz detection with a high dynamic range of 60 dB and large bandwidth up to 4.5 THz. The LT-GaAs metasurface has the potential to serve as a universal ultrafast switching element for THz applications, enabling low-cost, turn-key THz systems for a variety of real-world applications.

1. Introduction

The terahertz (THz) frequency band has enabled sensitive gas spectroscopy [1-3], advanced imaging [4, 5] and, more recently, high data rate short-range communications. [6, 7] Despite impressive advances in THz technologies, sensitive THz detectors remain a challenge, while compact THz sources such as quantum cascade lasers and resonant-tunneling diodes [8-12] are limited in the wavelength of operation and efficiency. As a result, many THz applications rely on ultrafast photoconductive antenna (PCA) detectors and sources gated by near-infrared lasers. Fiber-based lasers at telecom wavelengths (1.55 μm) are particularly attractive for gating photoconductive devices due to their high stability, robustness, compact footprint and reduced cost in comparison to Ti:Sapphire lasers. However, photoconductors such as InGaAs with bandgaps matching the photon energy of a telecom laser tend to exhibit low resistivity and long carrier lifetimes, which limit the sensitivity and bandwidth of detectors and the output power of sources. To mitigate these drawbacks, sophisticated material systems such as ion-implanted multilayer heterostructures [13-17] are required to make these materials viable for THz applications.

Interestingly, one of the best ultrafast photoconductive materials – low-temperature grown GaAs (LT-GaAs) – has been known to weakly absorb light at 1.55 μm despite its much larger bandgap (1.42 eV, ~870nm). Photon absorption at this wavelength has been explained as a two-step process

mediated by midgap states. [18, 19] This effect is small and therefore it is rarely used in practical devices, as it requires high optical gate powers and/or elaborate PCA designs such as optical cavities or plasmonic structures [20-22]. These additional metallic elements can enhance light absorption, but at the expense of ohmic losses, reduced dark resistance and low damage threshold.

Recent advances in all-dielectric metasurfaces have opened an alternative route for enhancing light absorption for materials with inherent low-absorption – even to the level of perfect (100%) absorption. Nanostructuring of the photoconductive material into a metasurface allows not only enhancing the effective absorption but also modifying of the electronic properties by geometrically defining a channel for charge transport. [23-27] Here, we use this approach to enhance the weak two-step photon absorption in LT-GaAs at 1.55 μm whilst also making use of its superior ultrafast photoconductive material properties for THz detection, namely short carrier lifetime, high dark resistivity and high electron mobility. The developed metasurface is then integrated into a PCA and is used for the detection of broadband THz pulses in a THz time-domain spectroscopy (TDS) system gated by a telecom wavelength laser (~1.55 μm). We demonstrate high sensitivity THz detection with a high dynamic range of 60 dB and large bandwidth up to 4.5 THz. This excellent detection performance combined with well-established LT-GaAs growth makes these metasurface-integrated THz detectors a viable alternative to PCAs based on InGaAs that require complex device architectures or schemes for modifying its lifetime. LT-GaAs metasurface-based detectors could therefore enable low-cost, turn-key THz systems for a variety of real-world applications such as THz sensing, medical imaging and communications.

2. Metasurface-Enhanced Sub-Bandgap Absorption

In theory, perfect (100%) photon absorption can be achieved in all-dielectric metasurfaces by critically coupling the incident field to two degenerate modes of opposite symmetry (odd and even). [28] It has been shown previously that optically thin LT-GaAs metasurfaces supporting two degenerate modes can be used to reach perfect absorption for wavelengths above the bandgap.[29, 30] However, implementing this approach for sub-bandgap absorption in LT-GaAs, for example at 1.55 μm, is significantly more challenging. Another difficulty lies in achieving high absorption and sub-picosecond

photocurrent response in the metasurface simultaneously. In this section, we first discuss the photoconductive metasurface concept and design (Section 2.1), and later describe how we address these challenges (Section 2.2).

2.1. Metasurface Design

To maximize absorption, we design a metasurface that supports two degenerate Mie modes of opposite symmetry at the laser excitation wavelength (**Figure 1**a). [29] The metasurface design can be understood by first considering a simple array of GaAs cubes (Inset of Figure 1c). When excited with linearly polarized light, the two lowest order Mie modes - the magnetic dipole (MD) mode and the electric dipole (ED) mode - are directly excited in each cube, albeit at different wavelengths. These modes have characteristic in-plane magnetic (electric) field vectors centered in the cubes and aligned predominantly along one direction. For the incident light linearly polarized light along the y-axis, the electric field vector of the ED mode is aligned close to the y-axis, and the magnetic field vector of the MD mode is aligned close to the x-axis. To support the flow of photogenerated charge carriers, the metasurface is then interconnected by adding continuous vertical channels between neighboring cubes. Following this, the metasurface design is modified to tune the ED and MD modes so that the two modes become degenerate and are centered at 1.55 µm. [29] Figure 1d shows the simulated magnetic and electric field distribution of the MD and ED modes in the x- and y-direction, respectively, when the modes are degenerate at 1.55 µm.

Each of the modes can be independently tuned in wavelength by choosing appropriate metasurface parameters that affect the wavelength of one mode while not significantly affecting the other. [29] For example, Figure 1c demonstrates how the ED resonance wavelength is tuned by simultaneously changing the width of the cube, *w* and horizontal periodicity (thereby maintaining a constant gap, *g*). In contrast, the MD mode remains practically unaffected by this change. When the two modes with opposite symmetries spectrally overlap, light absorption is enhanced, provided that there is some residual absorption of the constituent material at that wavelength (Fig. 1c, yellow circle).

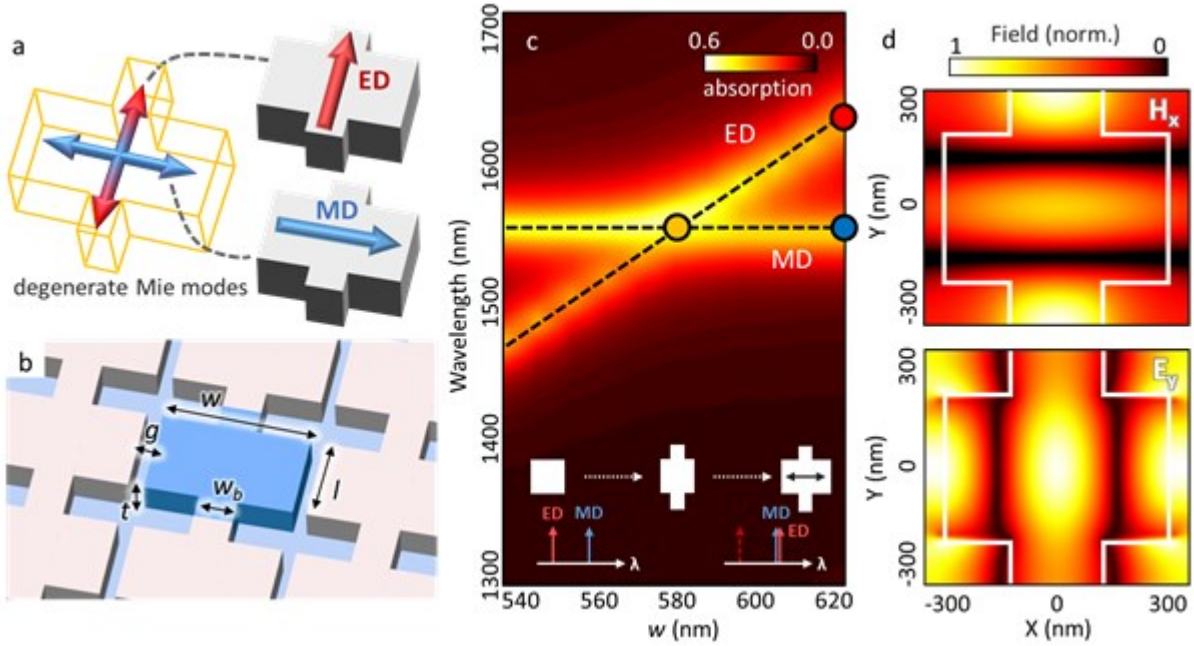

Figure 1. Photoconductive metasurface design. (a) Schematic diagram of the unit-cell supporting two degenerate modes, and (b) geometrical parameters of metasurface: w = 560 nm, l = 420 nm, t = 320 nm, w_b = 240 nm, g = 70 nm P_x = 630 nm, P_y = 690 nm. (c) Electric dipole (ED) mode tuning using the block width w. Inset: diagram of the design process showing two steps: metasurface interconnection and tuning the ED and magnetic dipole (MD) modes to the same wavelength. (d) Normalized magnetic and electric field distribution of the ED and MD modes respectively at ~1.55 μm (yellow circle in c). In (c) and (d) the LT-GaAs metasurface was simulated with a constant refractive index n = 3.37 and extinction coefficient κ = 0.01.

2.2. Enhancing sub-bandgap absorption for photoconductive THz detection

The first challenge in achieving high absorption with the LT-GaAs metasurface at 1.55 μm is the extremely weak and poorly-characterized material absorption at that wavelength. For perfect absorption, the two degenerate modes must be critically coupled to the incident field, meaning that the radiative loss of each mode, γ, matches its absorption loss, δ, i.e. $\gamma = \delta$ [28]. The lower the absorption loss (determined by the extinction coefficient, κ), the higher the precision in metasurface

design is required. However, the extinction coefficient for sub-bandgap absorption in LT-GaAs is not well known and it varies with the material growth conditions and annealing temperature. [31] Furthermore, due to the two-step absorption process, the material absorption in LT-GaAs at this wavelength increases non-linearly with the incident power. [18] We therefore make an initial estimate of $\kappa = 0.01$ using previous studies that report ~5% absorption of a 500 nm thick LT-GaAs layer pumped with 80 fs pulses at 1.57 µm with an average incident power of 50 mW. [32] We will show later how our experimental measurements are used to refine our estimate and arrive at a more accurate value for κ.

The second challenge in the metasurface design is to maintain a sub-picosecond photocurrent response while providing enhanced absorption. Given that the intrinsic absorption in LT-GaAs at 1.55 µm is very small, the condition of critical coupling at this wavelength demands very low radiative losses for the relevant modes (i.e. increasing the mode Q-factor). Low radiative losses can be achieved by tuning the width of the vertical bar w_b and gap size, g (shown in the supporting information). While this maximizes peak absorption, it also leads to a very narrow absorption band, which slows down the switching response time and it is therefore detrimental to broadband THz detection.

For best switching performance of the metasurface it is ideal to match the absorption linewidth to the spectral width of the ultrafast laser used for gating. This ensures a fast rise of the photoconductivity – albeit with a lower peak absorption level – as well as full use of the optical power. For this reason, we intentionally detune from the critical coupling condition and choose metasurface parameters which result in an absorption linewidth of approximately 50 nm, accepting an inevitable reduction in peak absorption.

3. Results & Discussion

3.1. Optical Metasurface Measurements

The chosen metasurface design (shown in Figure 1) was then fabricated using e-beam lithography and etching (see the Experimental Section for details). **Figure 2** shows scanning electron microscope (SEM) images of the fabricated metasurface and its measured optical transmission and reflection spectra.

The metasurface spectra (Figure 2c) show distinct peaks around 1.55 µm, corresponding to the Mie modes as designed in numerical simulations (Figure 2e). In comparison, the experimental spectra for the unpatterned LT-GaAs layer of the same thickness (320 nm) contains no resonant features, and only shows a weak variation with wavelength due to Fabry-Perot reflections within the layer (Figure 2d). The discrepancy between the measured and simulated spectra for the unpatterned layer in Figure 2d can be attributed to small differences in the fabricated and simulated LT-GaAs layer thickness.

The reflectivity and transmission spectra of the metasurface allow us to estimate absorption in the structure. The absorption spectrum exhibits a peak centered at 1.55 µm, reaching a maximum value of ~28% with a linewidth of approximately 35 nm (full width at half maximum (FWHM), Figure 2f). This absorption spectrum is in stark contrast to the spectrum of the LT-GaAs layer, which does not show any measurable absorption across the entire wavelength range. We note that the error in the experimental absorption values in Figure 2f is ~ 5%.

Despite the experimental error, the absorption peak in the LT-GaAs metasurface is striking in comparison to the unpatterned material. It demonstrates the powerful capabilities of the degenerate critical coupling scheme: absorption is strongly enhanced by nanostructuring the optically-thin photoconductor layer into a metasurface, and it is achieved without introducing additional elements such as back reflectors or plasmonic gratings. We note that due to a weak white light source used in the reflection/transmission measurements, the metasurface absorption could be considerably higher when excited with a pulsed laser source due to the nonlinear power dependency of LT-GaAs absorption. Our metasurface therefore can achieve an absorption enhancement sufficient for practical applications while providing an appropriate bandwidth for sub-picosecond switching.

We can now use these experimental results to infer values of the intrinsic absorption in LT-GaAs. The extinction coefficient can be more accurately estimated by simulating the metasurface for different values of κ (shown in Supporting Information) and comparing the peak absorption to the experimental results. We find the best agreement for a value of $\kappa = 0.003$. Figure 2e shows the corresponding simulated metasurface optical properties.

The experimental reflectivity and transmission spectra show a peak splitting, which is not present in simulations. The splitting is likely caused by either a small misalignment of the ED and MD

modes or excitation of an additional mode in the metasurface when illuminated by a focused beam used in the experiments. Despite the splitting feature, we find a good agreement between the simulated and experimental absorption spectra (Fig. 2e, f).

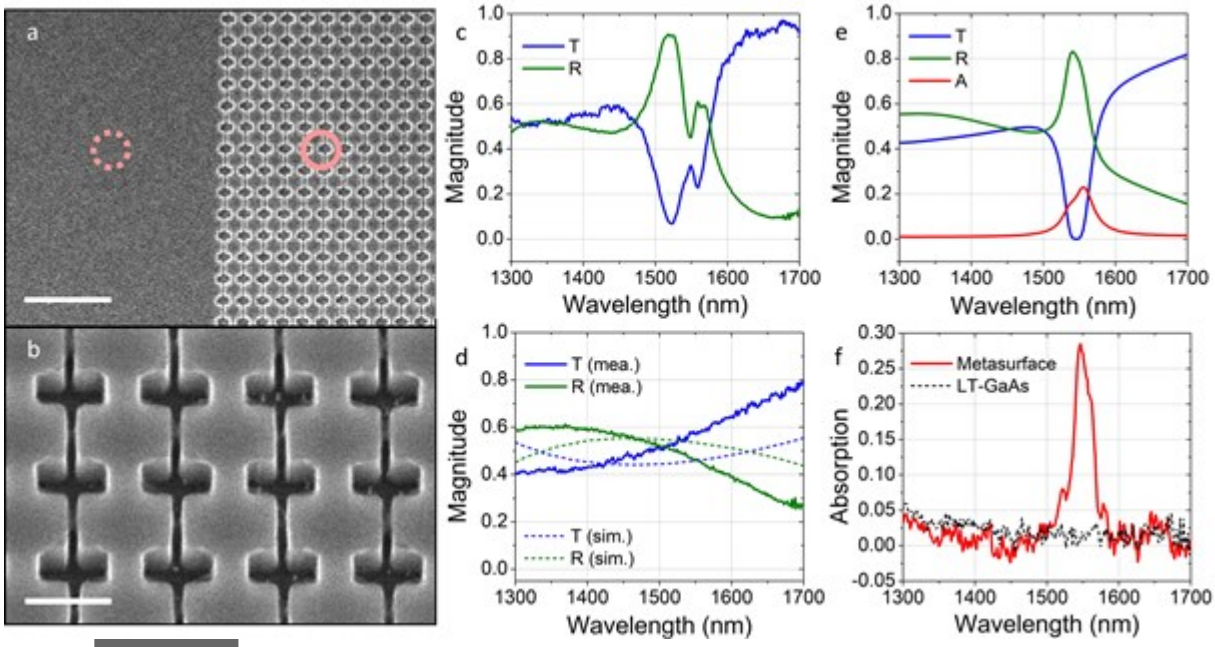

Figure 2. Simulated and experimental optical measurements of LT- GaAs metasurface. (a, b) SEM images of the LT-GaAs metasurface, scale bars: 2.5 µm (a) and 500 nm (b). Reflection and transmission spectra of (c) the metasurface (measured), and (d) unpatterned LT-GaAs (solid lines – measured, dashed lines – simulated). (e) Simulated transmission (T), reflection(R) and absorption (A) spectra of the LT-GaAs metasurface with extinction coefficient κ = 0.003. (f) Measured absorption spectra of the metasurface (red solid) and unpatterned LT-GaAs (black dashed).

3.2. THz detection with laser gating at 1.55 µm

After confirming that the metasurface enables considerable absorption for sub-bandgap excitation at ~1.55 µm within a 35 nm band, we examine the photoconductive response of the metasurface for THz detection. A metallic THz antenna with a 3 µm gap at the center is patterned directly on top of the

metasurface using e-beam deposition and lift-off process (**Figure 3**a). A 2 mm diameter silicon lens is attached to the substrate side to improve the THz collection efficiency. A standard TDS setup (Figure 3b) based on a 1.55 μm 100 fs-pulsed laser with a 76 MHz repetition rate is used to test the PCA as a THz detector. THz pulses are generated by exciting a 1 μm-thick InAs layer with laser pulses using an average power of 80 mW [32-34] (details of the experimental setup are shown in Supporting Information).

Figure 3c shows the detected THz waveform when the MS PCA detector is gated with 17 mW of average gate power, and the corresponding normalized power spectrum is shown in Figure 3d. The waveform shows a fast rise time of ~0.25 ps from the zero-field level to the peak, and a full width at half maximum (FWHM) of the field evolution of 0.3 ps (see Figure 3c). The fast variation of the detected field indicates that the sub-picosecond photocurrent response of the LT-GaAs is preserved in the metasurface detector. It should be noted that the observed response time is only an estimation as the measurement could be limited by the THz pulse itself. Another key parameter to evaluate the THz detection is dynamic range, which is defined as the ratio of the power density at the peak to the noise level. In Figure 3d, the measurement shows excellent detection performance, with high dynamic range of 60 dB with up to 4.5 THz bandwidth. A direct comparison of our detector with other PCA detectors gated by 1.55 μm light is difficult due to varying measurement conditions, such as the use of different THz sources and modulation schemes. Nevertheless, we estimate that the metasurface detector outperforms previously reported LT-GaAs-based detectors operating with 1.55 μm excitation in terms of dynamic range [18, 20, 35, 36] and it is comparable to state-of-the-art InGaAs-based detectors. [14, 16, 37-39]

We attribute the high dynamic range and the large bandwidth not only to the large absorption enabled by the metasurface at 1.55 μm, but also to the low dark current. The low value of dark current is a result of the drastically reduced photoconductive channel cross-section in the metasurface and the high resistivity of LT-GaAs. The ungated detector shows a resistance of 10 GΩ, several orders of magnitude higher than many reported PCAs based on advanced InGaAs material systems where the material was modified by ion-implantation, introduction of heterostructures and geometrical structuring to increase the resistivity. [14, 16, 37-39] We note that further improvements in dynamic range could be made with our LT-GaAs detector by using a more powerful THz source. Previously reported

PCA emitters (gated at λ=1.55 μm) were shown to produce as much as 3 orders of magnitude higher power in comparison to InAs emitters [40-42] used in this work.

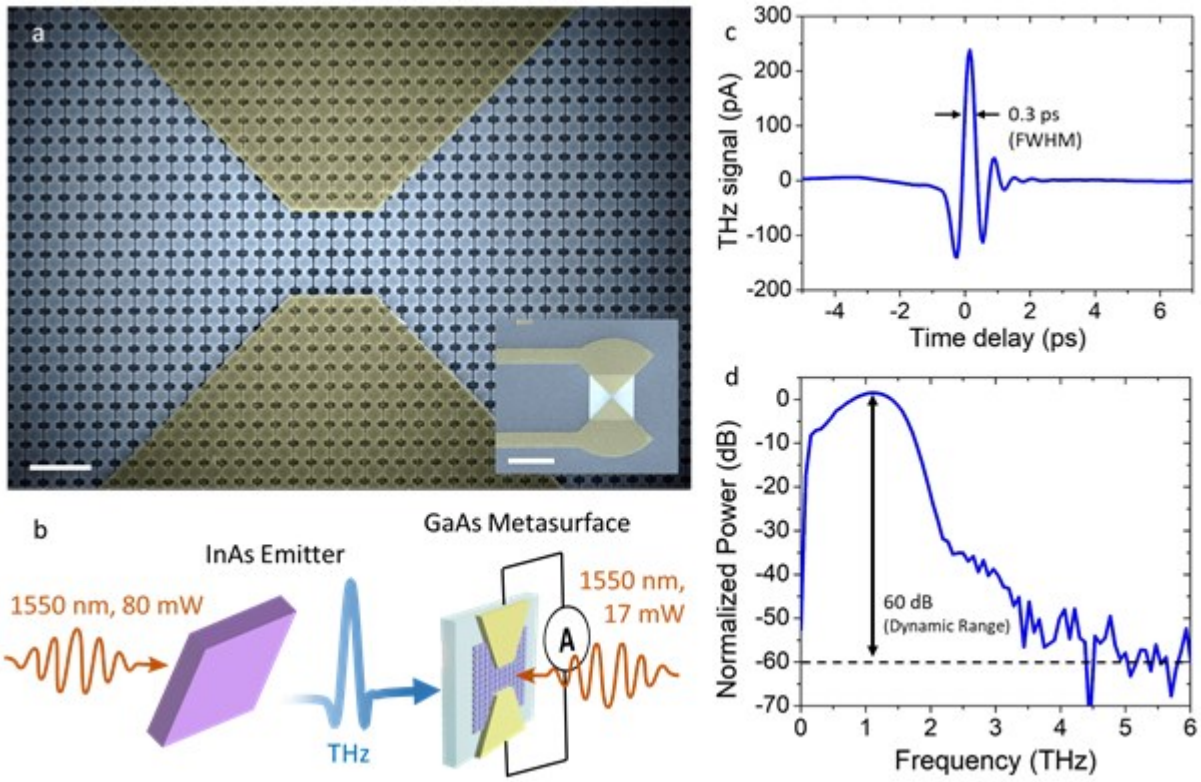

Figure 3. THz Detection with LT-GaAs metasurface photoconductive detector. (a) False color scanning electron microscope (SEM) image of the photoconductive channel with the metasurface integrated in the gap: (blue) LT-GaAs and (yellow) metallic antenna. Scale bar is 2 μm. Inset: THz antenna; scale bar is 30 μm. (b) Schematic diagram of experimental setup. (c) Detected time-domain waveform of the THz pulse generated from a 1 μm-thick InAs layer, and (d) its normalized Fourier transform power spectrum. FWHM: full-width at half maximum.

3.3. Optical Gate Power Dependence of THz Photocurrent

For optimal performance, standard THz PCA detectors should be operated using an optical gate power below or close to the saturation power. [18, 20, 43-45] However, for the non-linear two-step absorption

process, the standard definition of saturation power is not appropriate. Therefore, to verify the two-step absorption mechanism and determine the range of optical gate powers where the metasurface PCA provides optimal performance, we investigate THz detection for a range of gate powers and different THz field strengths.

In **Figure 4**, we show the THz amplitude as a function of the gate power for two detector samples without the collecting Si lens. A super-linear power dependence on gating power can be seen in the logarithmic plot. The peak THz amplitude, E_{THz}^{Peak}, follows a $P^{1.35}$ power-law for both samples (dashed lines). We also measured the power dependence for one of these detectors fitted with the Si lens. The lens focuses the THz wave producing approximately one order of magnitude higher THz field strength. The same super-linear power dependence was measured for the higher THz field strength. The observed power-law is consistent with earlier characterization of LT GaAs for sub-bandgap excitation, indicating that the photocurrent is indeed a result of absorption mediated by midgap states. [18]

The same power-law dependence for all gate power levels spanning almost three orders of magnitude and two different THz field strengths indicates that the LT-GaAs metasurface detector does not begin to saturate for the entire range of gate powers measured. This behavior is different from PCA detectors based on direct interband absorption where the standard linear dependence of the photocurrent saturates at gate powers of 0.1-10 mW, limiting the detection sensitivity at higher gating powers. [43] The experimental findings suggest that the sensitivity and dynamic range of LT-GaAs metasurface detectors could further improve at higher gate powers when gated by 1.55 µm lasers. More detailed investigations of the noise dependence on the gate power are therefore required to determine the optimum operation conditions of the metasurface detector, and to make a direct comparison to other detectors operating with 1.55 µm excitation.

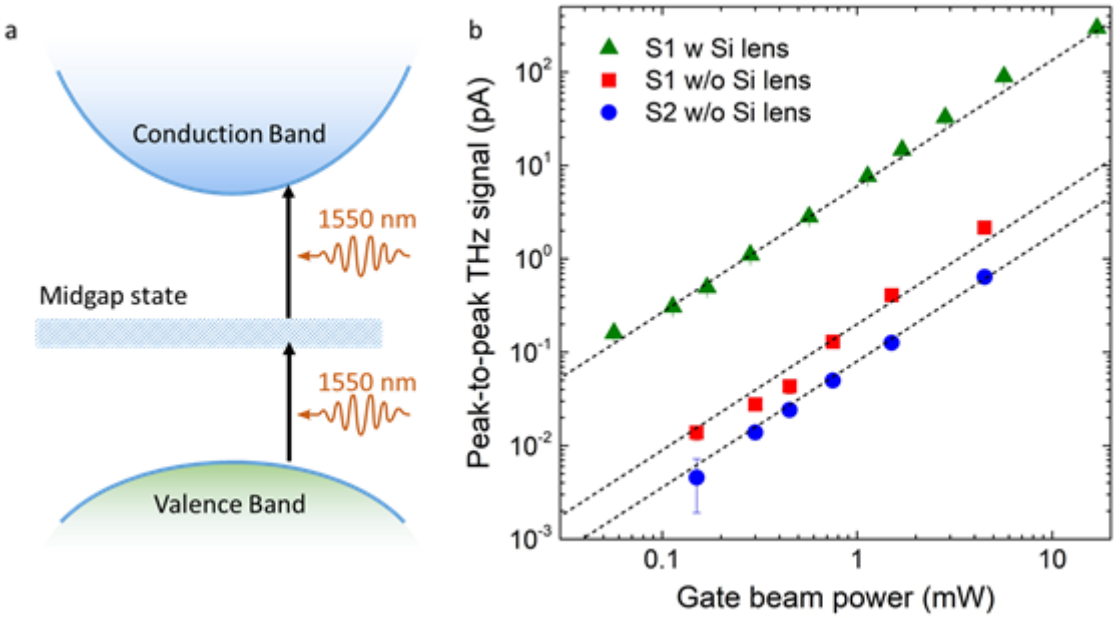

Figure 4. THz signal dependence on the gate power for LT-GaAs metasurface THz detector. (a) Schematic of the two-step photon absorption process enabled by midgap states in arsenic-rich LT-GaAs. (b) THz pulse peak-to-peak amplitude measured with two similar metasurface detectors without silicon lenses (blue circles, red squares) and a metasurface detector fitted with the silicon lens (green triangle), measured for varying laser gating power. Black dashed lines show the $E_{THz}^{Peak} \propto P^{1.35}$ power dependence.

4. Conclusion

In conclusion, we have demonstrated that LT-GaAs metasurfaces can be used for sensitive photoconductive THz detection when gated by telecom-wavelength lasers operating in the 1.55 µm wavelength band. Using the concept of perfect absorption via degenerate critical coupling, LT-GaAs is nanostructured into a metasurface which significantly enhances the weak sub-bandgap photon absorption due to midgap states. The metasurface improves the laser photon to charge carrier conversion efficiency to the level sufficient for practical applications, whilst the LT-GaAs material platform provides high dark resistance, high electron mobility and short photocarrier lifetime required for THz detection. Excellent detection performance is achieved without the use of plasmonic elements

which tend to increase complexity of the device and decrease the damage threshold. In addition, the metasurface geometry provides direct control of the wavelength of operation and the photoconductive channel properties, enabling integration with a wide range of THz platforms. The full potential of the LT-GaAs metasurface detectors with 1.55 µm excitation can be realized by simultaneously optimizing LT-GaAs electronic properties [30, 37] and the metasurface design. Nevertheless, the results shown here already demonstrate that metasurface detectors using LT-GaAs can operate not only with direct inter-band excitation, but also with sub-bandgap excitation using low-cost and robust telecom lasers. LT-GaAs photoconductive metasurfaces are therefore a viable alternative to the ultrafast InGaAs-based material systems and have the potential to serve as a universal ultrafast switching element for THz applications.

5. Experimental Section

Sample Fabrication: A 320-nm-thick LT-GaAs layer and two $Al_{0.55}Ga_{0.45}As$ stop-etch layers with 100-nm-thick GaAs spacer are grown on a (100)-oriented GaAs wafer (VB1113). To define a metasurface on the LT-GaAs layer, e-beam lithography process is conducted with ZEP 520A e-beam resist. Then, the LT-GaAs metasurface structures are formed by inductively coupled plasma reactive ion etching process with mixture of BCl_3, Cl_2, Ar, and N_2 gases (10, 10, 10, and 3.5 cm^3/min, respectively). The fabricated sample is bonded on the 500-µm-thick sapphire substrate using epoxy (353ND, EPO-TEK) and the backside GaAs wafer is removed using mechanical lapping and a wet-etch process.[26] For the wet-etching process, we use a citric acid etchant (citric acid : H_2O_2 = 5 : 1) to etch the GaAs substrate and the spacer, and a phosphoric acid etchant (H_3PO_4 : H_2O : H_2O_2 = 20 : 200 : 4) is used to etch the $Al_{0.55}Ga_{0.45}As$ stop-etch layer. After the fabrication, only the LT-GaAs metasurface is left on the transparent sapphire substrate. To make a metasurface THz detector, we integrate two metallic electrodes shaped as a THz antenna over the metasurface (Fig. 1). The antenna has a 3 µm gap between the electrode tips and it is fabricated with 300-nm thick metallic alloy (Ni/Ge/Au/Ni/Au) using e-beam deposition and lift-off process.

Numerical Simulations: The numerical simulations of the metasurface shown in Figure 1 of the main text were carried out using commercial finite-difference time domain (FDTD) software Lumerical. A unit cell of the metasurface is simulated with periodic boundary conditions in the x- and y- directions and perfectly matched layer (PML) boundaries in the z-direction. The metasurface is simulated as being embedded in a constant refractive index no-loss material (n = 1.56) to simulate epoxy. The half-space below the metasurface is also simulated as epoxy and the region above the metasurface top surface is simulated as air (n =1). The metasurface is excited from below (through the epoxy) by a plane wave to match experimental conditions. The LT-GaAs metasurface itself is simulated as having a constant refractive real refractive index of n = 3.37, which reflects the refractive index of LT-GaAs at 1.55 µm. As discussed in Section 2.2 of the main text, the extinction coefficient of LT-GaAs is not well characterized, and an initial estimate from the literature of κ = 0.01 was used for the simulation results in Figure 1. In Figure 2e, an extinction coefficient of κ = 0.003 was used to reflect experimental measurements (see Supporting Information).

Linear transmission measurements: We used a home-built spectroscopy system with white light illumination from a fiber-coupled incandescent lamp. The light beam is focused on the sample by a convex lens (focal length = 25 mm, numerical aperture = 0.12) at normal incidence. The transmitted beam is collected by an identical lens on the other side of the sample. Then, the reflected and transmitted light is analyzed using an infrared spectrometer (NIRquest, Ocean Optics). The measured transmission and reflection spectra are normalized using reference measurements on a sapphire substrate (without the metasurface) and on a silver mirror, respectively. Details of optical spectra calculation is in Supporting Information.

Supporting Information

Supporting Information is available from the Wiley Online Library or from the author.

Acknowledgements

This work was supported by the U.S. Department of Energy, Office of Basic Energy Sciences, Division of Materials Sciences and Engineering. LLH was supported by the EPSRC (EP/P021859/1, EP/L015455/1, EP/T517793/1). Metasurface fabrication and characterization were performed at the Center for Integrated Nanotechnologies, an Office of Science User Facility operated for the U.S. Department of Energy (DOE) Office of Science. Sandia National Laboratories is a multi-mission laboratory managed and operated by National Technology and Engineering Solutions of Sandia, LLC., a wholly owned subsidiary of Honeywell International, Inc., for the U.S. Department of Energy's National Nuclear Security Administration under contract DE-NA-0003525. This article describes objective technical results and analysis. The views expressed in the article do not necessarily represent the views of the U.S. DOE or the United States Government.

Received: ((will be filled in by the editorial staff))
Revised: ((will be filled in by the editorial staff))
Published online: ((will be filled in by the editorial staff))

References

[1] M. Seo, H.-R. Park, *Adv. Opt. Mater.* **2020**, 8, 1900662.

[2] Y.-D. Hsieh, S. Nakamura, D. G. Abdelsalam, T. Minamikawa, Y. Mizutani, H. Yamamoto, T. Iwata, F. Hindle, T. Yasui, *Sci. Rep.* **2016**, 6, 28114.

[3] L. Yang, T. Guo, X. Zhang, S. Cao, X. Ding, *Rev. Anal. Chem.* **2018**, 37, 20170021.

[4] I. Duling, D. Zimdars, *Nat. Photon.* **2009**, 3, 630-632.

[5] D. M. Mittleman, *Opt. Express* **2018**, 26, 9417-9431.

[6] L. Tohmé, S. Blin,G. Ducournau, P. Nouvel, D. Coquillat, S. Hisatake, T. Nagatsuma, A. Pénarier, L. Varani, W. Knap, J.-F. Lampin, *Electron. Lett.* **2014**, 50, 323-325.

[7] T. Nagatsuma, G. Ducournau, C. C. Renaud, *Nat. Photon.* **2016**, 10, 371-379.

[8] Y. Zeng, B. Qiang, Q. J. Wang, *Adv. Opt. Mater.* **2020**, 8, 1900573.

[9] M. A. Kainz, M. P. Semtsiv, G. Tsianos, S. Kurlov, W. T. Masselink, S. Schönhuber, H. Detz, W. Schrenk, K. Unterrainer, G. Strasser, A. M. Andrews, *Opt. Express* **2019**, 27, 20688-20693.

[10] A. Forrer, M. Franckié, D. Stark, T. Olariu, M. Beck, J. Faist, G. Scalari, *ACS Photon.* **2020**, 7, 784-791.

[11] A. Al-Khalidi, K. H. Alharbi, J. Wang, R. Morariu, L. Wang, A. Khalid, J. M. L. Figueiredo, E. Wasige, *IEEE Trans. Terahertz Sci. Tech.* **2020**, 10, 150-157.

[12] K. Kasagi, S. Suzuki, M. Asada, *J. Appl. Phys.* **2019**, 125, 151601.

[13] I. Kostakis, D. Saeedkia, M. Missous, *IEEE Trans. Terahertz Sci. Tech.* **2012**, 2, 617-622.

[14] R. B. Kohlhaas, S. Breuer, S. Nellen, L. Liebermeister, M. Schell, M. P. Semtsiv, W. T. Masselink, B. Globisch, *Appl. Phys. Lett.* **2019**, 114, 221103.

[15] R. B. Kohlhaas, R. J. B. Dietz, S. Breuer, S. Nellen, L. Liebermeister, M. Schell, B. Globisch, *Opt. Lett.* **2018**, 43, 5423-5426.

[16] B. Globisch, R. J. B. Dietz, R. B. Kohlhaas, T. Göbel, M. Schell, D. Alcer, M. Semtsiv, W. T. Masselink, *J. Appl. Phys.* **2017**, 121, 053102.

[17] M. Suzukia, M. Tonouchi, *Appl. Phys. Lett.* **2005**, 86, 163504.

[18] M. Tani, K.-S. Lee, X.-C. Zhang, *Appl. Phys. Lett.* **2000**, 77, 1396.

[19] N. Vashistha, M. Kumar, R. K. Singh, D. Panda, L. Tyagi, S. Chakrabarti, *Physica B Condens. Matter* **2021**, 602, 412441.

[20] A. Jooshesh, V. Bahrami-Yekta, J. Zhang, T. Tiedje, T. E. Darcie, R. Gordon, *Nano Lett.* **2015**, 15, 8306-8310.

[21] F. Fesharaki, A. Jooshesh, V. Bahrami-Yekta, M. Mahtab, T. Tiedje, T. E. Darcie, R. Gordon, *ACS photon.* **2017**, 4, 1350-1354.

[22] M. Billet, P. Latzel, F. Pavanello, G. Ducournau, J.-F. Lampin, E. Peytavitb, *APL Photon.* **2016**, 1, 076102.

[23] C.-C. Chang, W. J. M. Kort-Kamp, J. Nogan, T. S. Luk, A. K. Azad, A. J. Taylor, D. A. R. Dalvit, M. Sykora, H.-T. Chen, *Nano Lett.* **2018**, 18, 7665-7673.

[24] A. K. Azad, W. J. M. Kort-Kamp, M. Sykora, N. R. Weisse-Bernstein, T. S. Luk, A. J. Taylor, D. A. R. Dalvit, H.-T. Chen, *Sci. Rep.* **2016**, 6, 20347.

[25] X. Xu, H. Kwon, B. Gawlik, N. M. Estakhri, A. Alù, S. V. Sreenivasan, A. Dodabalapur, *Nano Lett.* **2018**, 18, 3362-3367.

[26] T. Siday, P. P. Vabishchevich, L. Hale, C. T. Harris, T. S. Luk, J. L. Reno, I. Brener, O. Mitrofanov, *Nano Lett.* **2019**, 19, 2888-2896.

[27] O. Mitrofanov, T. Siday, R. J. Thompson, T. S. Luk, I. Brener, J. L. Reno, *APL Photon.* **2018**, 3, 051703.

[28] R. Alaee, M. Albooyeh, C. Rockstuhl, *J. Phys. D: Appl. Phys*. **2017**, 50, 503002.

[29] O. Mitrofanov, L. L. Hale, P. P. Vabishchevich, T. S. Luk, S. J. Addamane, J. L. Reno, I. Brener, *APL Photon.* **2020**, 5, 101304.

[30] L. L. Hale, P. P. Vabishchevich, T. Siday, C. T. Harris, T. S. Luk, S. J. Addamane, J. L. Reno, I. Brener, O. Mitrofanov, *Opt. Express* **2020**, 28, 35284.

[31] C. Tannoury, M. Billet, C. Coinon, J-F. Lampin, E. Peytavit, *Electron. Lett.* **2020**, 56, 17, 897–899.

[32] A. Jooshesh, F. Fesharaki, V. Bahrami-Yekta, M. Mahtab, T. Tiedje, T. E. Darcie, R. Gordon, *Opt. Express* **2017**, 25, 22140-22148.

[33] M. Reid, I. V. Cravetchi, R. Fedosejevs, *Phys. Rev. B* **2005**, 72, 035201.

[34] S. Ono, T. Tsukamoto, E. Kawahata, T. Yano, H. Ohtake, N. Sarukura, *Appl. Opt.* **2001**, 40, 1369-1371.

[35] T. Kataoka, K. Kajikawa, J. Kitagawa, Y. Kadoya, Y. Takemura, *Appl. Phys. Lett.* **2010**, 97, 201110.

[36] J.-M. Rämer, F. Ospald, G. von Freymann, R. Beigang, *Appl. Phys. Lett.* **2013**, 103, 021119.

[37] H. Erlig, S. Wang, T. Azfar, A. Udupa, H. R. Fetterman, D. C. Streit, *Electron. Lett.* **1999**, 35, 173-174.

[38] U. Nandi, J. C. Norman, A. C. Gossard, H. Lu, S. Preu, *J. Infrared Milli. Terahz. Waves* **2018**, 39, 340-348.

[39] H. Roehle, R. J. B. Dietz, H. J. Hensel, J. Böttcher, H. Künzel, D. Stanze, M. Schell, B. Sartorius, *Opt. Express* **2010**, 18, 2296-2301.

[40] M. L. Smith, R. Mendis, R. E. M. Vickers, R. A. Lewis, *J. Appl. Phys*. **2009**, 105, 063109

[41] B. Globisch, R. J. B. Dietz, T. Göbel, M.Schell, W. Bohmeyer, R. Müller, A. Steiger, *Opt. Lett.* **2015**, 40, 3544-3547.

[42] R. J. B. Dietz, B. Globisch, M. Gerhard, A. Velauthapillai, D. Stanze, H. Roehle, M. Koch, T. Gobel, M. Schell, *Appl. Phys. Lett.,* **2013**, 103, 061103

[43] L. L. Hale, C. T. Harris, T.S. Luk, S. J. Addamane, J. L. Reno, I.Brener, O. Mitrofanov, *Opt. Lett.* **2021**, 46, 3159-3162.

[44] S. Rihani, R.Faulks, H. Beere, H. Page, I. Gregory, M. Evans, D. A. Ritchie, M. Pepper, *Appl. Phys. Lett.* **2009** 96, 051106.

[45] R. Yano, H. Gotoh, Y. Hirayama, S. Miyashita, Y. Kadoya, T. Hattori, *J. Appl. Phys.* **2015**, 97, 103103

Table of Contents

Low-temperature grown gallium arsenide (LT-GaAs) is one of the best photoconductive materials for detecting terahertz radiation. However, the large bandgap of LT-GaAs prevents its use with robust telecom lasers. This work presents a photoconductive LT-GaAs metasurface which uses the concept of perfect absorption to strongly enhance a very weak two-step optical absorption at 1.55 μm via midgap states, enabling sensitive terahertz detection.

H. Jung*, L. L. Hale*, J. Briscoe, R. Sarma, T. S. Luk, S. J. Addamane, J. L. Reno, I. Brener, O. Mitrofanov*

Terahertz detection using enhanced two-step absorption in photoconductive metasurfaces